

Heterogeneous Catalysis
How to cite: *Angew. Chem. Int. Ed.* **2020**, 59, 22763–22770

International Edition: doi.org/10.1002/anie.202007228

German Edition: doi.org/10.1002/ange.202007228

Raising the CO_x Methanation Activity of a Ru/ γ -Al₂O₃ Catalyst by Activated Modification of Metal–Support Interactions

Shilong Chen, Ali M. Abdel-Mageed,* Michael Dyballa, Magdalena Parlinska-Wojtan, Joachim Bansmann, Simone Pollastri, Luca Olivi, Giuliana Aquilanti, and R. Jürgen Behm*

Abstract: Ru/Al₂O₃ is a highly stable, but less active catalyst for methanation reactions. Herein we report an effective approach to significantly improve its performance in the methanation of CO₂/H₂ mixtures. Highly active and stable Ru/ γ -Al₂O₃ catalysts were prepared by high-temperature treatment in the reductive reaction gas. Operando/in situ spectroscopy and STEM imaging reveals that the strongly improved activity, by factors of 5 and 14 for CO and CO₂ methanation, is accompanied by a flattening of the Ru nanoparticles and the formation of highly basic hydroxylated alumina sites. We propose a modification of the metal–support interactions (MSIs) as the origin of the increased activity, caused by modification of the Al₂O₃ surface in the reductive atmosphere and an increased thermal mobility of the Ru nanoparticles, allowing their transfer to modified surface sites.

Introduction

The methanation of CO₂ has attracted enormous interest recently, both as a possible means for curbing greenhouse gases and to chemically store excess electric energy from fluctuating renewable sources, which was discussed and considered as an important part of “power-to-gas” con-

cepts.^[1–3] Supported Ni catalysts are generally considered as standard catalyst for this reaction, but they are little active at low temperature (< 300 °C) and also suffer from deactivation due to sintering via Ni(CO)₄ formation.^[4,5] Supported Ru catalysts, which are more active and stable at lower temperatures, are therefore an attractive alternative for applications where lower temperatures are beneficial, despite of their higher costs.^[3,4] It quickly turned out that also the nature of the oxide support plays an important role,^[6] with a superior activity for Ru nanoparticles (NPs) supported on reducible oxides (TiO₂ or CeO₂)^[7] compared to much less active catalysts based on inert oxides such as Al₂O₃.^[8,9] Because of their significantly higher stability during reaction, however, Ru/Al₂O₃ catalysts would be an attractive alternative, provided their activity could be enhanced to the level of Ru/TiO₂. We demonstrated recently that the activity of Ru/TiO₂ catalysts for CO₂ methanation could be significantly improved by a high temperature reaction treatment in reductive atmosphere, which we had attributed to a modification of the metal–support interactions (MSIs),^[10] for example, by stabilization of metal NPs and/or charge transfer effects.^[6,11,12] Variation in the catalytic performance due to modification of MSIs has been considered for decades for noble metal catalysts supported on reducible oxides under reductive reaction conditions,^[13–16] including also CO₂ hydrogenation,^[10,17,18] but not for stable (inert) oxides such as Al₂O₃.^[6] Recent experimental and theoretical studies, however, indicated a stabilization of noble metals on penta-coordinated Al³⁺ sites, reflecting a modification of the MSIs that could lead also to the formation of flat NPs.^[19–21] This and also the hydroxylation of alumina were postulated to affect the CO₂ dissociation.^[20] Stimulated by these earlier findings and proposals we decided to explore the possibility of modifying the MSIs in a Ru/ γ -Al₂O₃ catalyst by a high-temperature treatment in the reaction gas atmosphere, employing a combination of in situ/ operando FTIR and X-ray absorption spectroscopy (XAS) measurements, coupled with CO/ pyrrole adsorption measurements and ex situ techniques for catalyst characterization. If successful, this work will not only introduce a new and efficient approach for fabricating highly active and stable Ru/ γ -Al₂O₃ catalysts for CO_x methanation, but also lead to a significantly improved fundamental understanding of the role of MSIs in metal catalysts supported on irreducible oxides.


[*] Dr. S. Chen, Dr. A. M. Abdel-Mageed, Dr. J. Bansmann, Prof. Dr. R. J. Behm
 Institute of Surface Chemistry and Catalysis, Ulm University
 89069 Ulm (Germany)
 E-mail: ali.abdel-mageed@uni-ulm.de
 juergen.behm@uni-ulm.de


Dr. M. Dyballa
 Institute of Technical Chemistry, Stuttgart University
 70569 Stuttgart (Germany)

Dr. M. Parlinska-Wojtan
 Institute of Nuclear Physics, Polish Academy of Sciences
 31-342 Krakow (Poland)

Dr. S. Pollastri
 CERIC-ERIC
 s. s. 14, km 163.5, 34149 Trieste, Basovizza (Italy)

Dr. L. Olivi, Dr. G. Aquilanti
 Elettra-Sincrotrone Trieste
 s. s. 14, km 163.5, 34149 Trieste, Basovizza (Italy)

 Supporting information and the ORCID identification number(s) for the author(s) of this article can be found under:
<https://doi.org/10.1002/anie.202007228>.

 © 2020 The Authors. Published by Wiley-VCH GmbH. This is an open access article under the terms of the Creative Commons Attribution Non-Commercial License, which permits use, distribution and reproduction in any medium, provided the original work is properly cited, and is not used for commercial purposes.

Results and Discussion

Ru/ γ -Al₂O₃ catalysts with ≈ 2.3 wt.% Ru loading were prepared by incipient wetness impregnation.^[6] We first evaluated the activity of the Ru/ γ -Al₂O₃ catalyst in the methanation of CO₂ in a CO₂/H₂ mixture (CO₂-ref: 15.5% CO₂, 80.9% H₂, N₂ balance) at 190 °C for 1000 min (190 °C-1 phase). Next we stepwise increased the temperature from 210 to 350 °C in a temperature programmed reaction (TPR) sequence, followed by a second reaction phase at 190 °C (190 °C-2 phase) for 1000 min (Experimental section, Supporting Information (SI)). In the 190 °C-1 phase, the catalyst showed a stable CO₂ methanation activity with a rate of $\approx 2.7 \mu\text{mol}_{\text{CH}_4} \text{g}_{\text{Ru}}^{-1} \text{s}^{-1}$ (TOF: $4.0 \times 10^{-4} \text{s}^{-1}$) and 100% selectivity for methane formation, with no evidence for the formation of gaseous CO via the reverse water-gas shift (RWGS) reaction. During the TPR sequence, the CO₂ conversion increased with temperature, reaching 61% at 350 °C, while keeping its high selectivity for methane formation (Figure 1a). Interestingly, after cooling down to 190 °C-2 phase, the catalyst showed a much higher activity ($40.5 \mu\text{mol}_{\text{CH}_4} \text{g}_{\text{Ru}}^{-1} \text{s}^{-1}$) than in the 190 °C-1 phase, while keeping essentially 100% selectivity for methane formation (Figure 1b). After less than 5% deactivation over 200 min on stream, the steady-state activity in the 190 °C-2 phase leveled off at $\approx 38.3 \mu\text{mol}_{\text{CH}_4} \text{g}_{\text{Ru}}^{-1} \text{s}^{-1}$ (TOF: $6.8 \times 10^{-3} \text{s}^{-1}$), which is ≈ 14 times higher than in the 190 °C-1 phase.

To unravel the influence of trace impurities of CO on CO₂ hydrogenation, we examined the CO₂ methanation in the

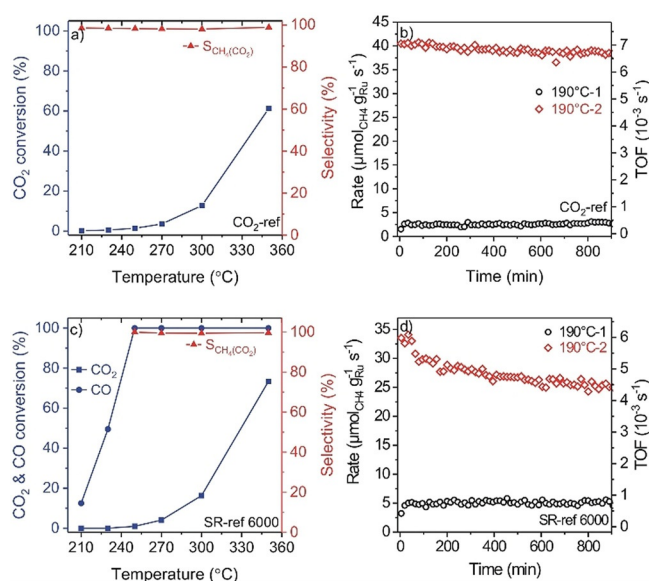


Figure 1. a) CO₂ conversion and selectivity for methane formation ($S_{\text{CH}_4(\text{CO}_2)} = R_{\text{CH}_4(\text{CH}_4 \text{ formation})} / R_{(\text{CO}_2 \text{ consumption})}$) in CO₂-ref in the range 210 to 350 °C. b) Temporal evolution of the Ru-mass-normalized CO₂ methanation rate and the corresponding TOFs in CO₂-ref reformat gas during isothermal reaction in the 190 °C-1 and 190 °C-2 phases. c) CO/CO₂ conversion and the selectivity for CO₂ methanation (see above) during reaction in SR-ref 6000 reformat gas in the range 210 to 350 °C. d) Temporal evolution of the Ru-mass-normalized CO methanation rate and the corresponding TOFs during reaction in SR-ref 6000 reformat gas in the 190 °C-1 and 190 °C-2 phases.

presence of CO traces (SR-ref 6000: 15.5% CO₂, 0.6% CO, 80.9% H₂, N₂ balance). During the 190 °C-1 phase, the catalyst showed only CO methanation (no CO₂ conversion), with a rather low rate of $\approx 5.0 \mu\text{mol}_{\text{CH}_4} \text{g}_{\text{Ru}}^{-1} \text{s}^{-1}$ (TOF: $7.6 \times 10^{-4} \text{s}^{-1}$) for 1000 min. The inhibition of CO₂ methanation under these conditions was previously explained and discussed in detail by CO_{ad} induced site blocking effects.^[22,23] During the TPR sequence, full CO conversion was reached at 250 °C (Figure 1c). At that point, CO₂ methanation started and increased with temperature, reaching a conversion of ≈ 73 % at 350 °C, with close to 100% selectivity towards methane formation (no RWGS activity). After cooling back to 190 °C-2, we did not see any evidence for CO₂ methanation. The increase in CO₂ methanation activity during the TPR sequence is largely similar to that observed in CO₂-ref reformat gas (in the absence of CO), indicating that the under these conditions the CO traces do not affect the CO₂ methanation behavior. Furthermore, we observed a ≈ 5 times higher CO methanation rate in the 190 °C-2 phase compared to that in the 190 °C-1 phase (Figure 1d). This higher rate is comparable to that reported on Ru/TiO₂ and Ru/zeolite catalysts, so far the most active Ru-based catalysts for (selective) CO methanation,^[8,23–25] but with a significantly higher stability of the Ru/ γ -Al₂O₃ catalyst (Table S1, SI).

To examine the impact of CO₂ on the observed enhancement of the CO methanation activity, we tested the CO methanation behavior in a CO₂-free gas mixture (ID-ref 6000: 0.6% CO, 80.9% H₂, N₂ balance). This test showed an essentially similar behavior as for the CO methanation in the SR-ref 6000 gas mixture, with little difference in the Ru-mass-normalized rates (see details in Figure S1, SI). Overall, the TPR sequence results in a pronounced enhancement both of CO₂ and CO methanation rates on Ru/ γ -Al₂O₃ catalyst, while CO traces do not measurably affect the CO₂ methanation performance.

To elucidate the physical origin of these changes in reactivity, we characterized the structural properties of the Ru/ γ -Al₂O₃ catalyst after the 190 °C-1 phase in SR-ref 6000 reformat (Ru/ γ -Al₂O₃-ISO), and after the TPR sequence and the subsequent 190 °C-2 phase (Ru/ γ -Al₂O₃-TPR), respectively.

XRD measurements indicated that the cubic γ -Al₂O₃ phase is retained after the TPR sequence, without any measurable bulk structural changes. The diffraction patterns did not show any Ru reflections, as expected for the very small Ru NPs in these catalysts (Figure S2, SI). Also the specific surface areas ($127 \pm 4 \text{ m}^2 \text{g}^{-1}$) and porosity (volume: $0.91 \text{ cm}^3 \text{g}^{-1}$, pore diameter: 22 nm) remained unchanged, confirming the stability of the γ -Al₂O₃ bulk structure during the TPR sequence (Table S2, SI). The structure of γ -Al₂O₃ was also examined by ²⁷Al magic angle sample spinning (MAS) NMR spectroscopy, after calcination and after the 190 °C-1 and 190 °C-2 phases (Figure S3, SI). We can clearly identify the Al³⁺ ions in octahedral (A_o, 7 ppm) and tetrahedral (A_t, 63 ppm) coordination sites on the three catalysts, while the concentration of pentahedral Al³⁺ sites (Al_p) was below the detection limit of the NMR measurements.^[19] Comparison of the NMR spectra indicated no significant

changes in the spectra, indicating that there is no measurable change in the coordination environment of Al^{3+} .

Furthermore, the structure of the catalysts was examined by (S)TEM (Figure 2a,c). Comparison of HAADF-STEM images recorded before and after the TPR sequence reveals the presence of very small Ru NPs with sizes in the range of 1–5 nm (see also Figure S4, SI). Ru particle size distributions, obtained by evaluating over 600 NPs in (S)TEM images (Figure 2b,d), revealed a slight increase of the mean Ru particle size from 1.5 ± 0.4 nm for the $\text{Ru}/\gamma\text{-Al}_2\text{O}_3\text{-ISO}$ catalyst to 1.7 ± 0.5 nm for the $\text{Ru}/\gamma\text{-Al}_2\text{O}_3\text{-TPR}$ catalyst. (S)TEM measurements performed after reaction in CO_2 -ref gas mixture under similar reaction conditions revealed mean particle sizes for the two catalysts (Figure S5, SI), which are essentially identical to those obtained after reaction in SR-ref 6000 reformat gas. Hence, the presence of CO in the feed gas (in SR-ref 6000) has little effect on the size/distribution of the Ru NPs after CO_2 hydrogenation.

Furthermore, we evaluated the shape of the Ru NPs by analyzing more than 600 Ru NPs on the (S)TEM images, following an approach described earlier.^[6,11,12] Briefly, this is based on determining the ratio of the shortest diameter (R_1) to the longest diameter (R_2) of the two-dimensional projection of each Ru NP (Figure 3a). Low R_1/R_2 ratios are expected for flat particles. Those particles observed from the side appear with an elliptic shape, while those viewed from the top should appear circular (Figure 3b,d). Spherical particles, in contrast, should always appear with circular projection, independent of the imaging angle (Figure 3b). The fraction of Ru particles with a ratio ≤ 0.8 was about 42% in the $\text{Ru}/\gamma\text{-Al}_2\text{O}_3\text{-ISO}$ catalyst (Figure 3c), while for $\text{Ru}/\gamma\text{-Al}_2\text{O}_3\text{-TPR}$ this increased to $\approx 69\%$ (Figure 3e), indicating an irreversible flattening of the Ru NPs during the TPR sequence. Further information on TPR induced changes of the Ru NPs was obtained from diffuse reflectance FTIR (DRIFTS) spectroscopy measurements during CO adsorption at 30°C . Both before and after the TPR sequence the catalysts

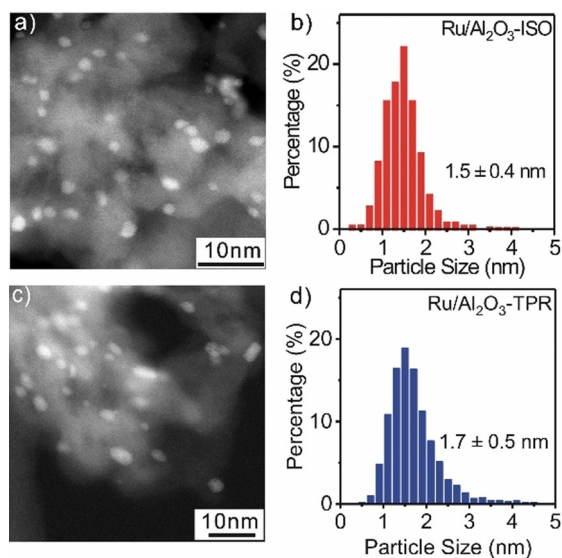


Figure 2. Representative HAADF-STEM images and Ru particle size distributions. a),b) $\text{Ru}/\gamma\text{-Al}_2\text{O}_3\text{-ISO}$ and c),d) $\text{Ru}/\gamma\text{-Al}_2\text{O}_3\text{-TPR}$ catalysts.

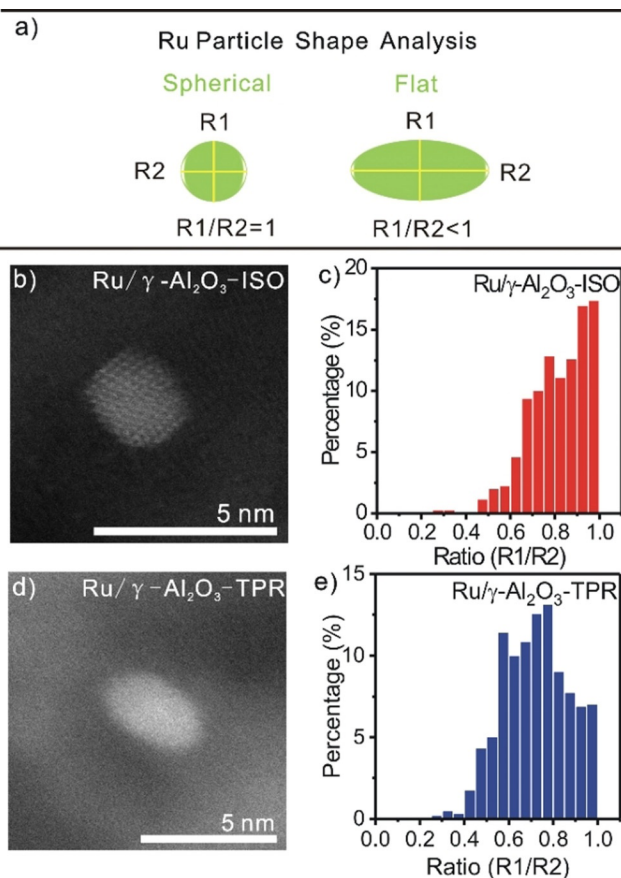


Figure 3. Ru particle shape analysis probed by (S)TEM. Schematic illustration of the particle shape analysis based on the TEM images (a). Representative HAADF-STEM images of the $\text{Ru}/\gamma\text{-Al}_2\text{O}_3\text{-ISO}$ (b) and $\text{Ru}/\gamma\text{-Al}_2\text{O}_3\text{-TPR}$ (d) catalysts, and diameter ratio distributions of the respective catalysts (c,e). Additional representative (S)TEM images used for size and shape evaluation are shown in Figure S4, Supporting Information.

showed typical bands of CO_{ad} species in the range from 1900 to 2170 cm^{-1} (Figure 4a). Assuming similar cross-sections for different CO_{ad} species, the CO_{ad} coverage on the Ru NPs in $\text{Ru}/\gamma\text{-Al}_2\text{O}_3\text{-TPR}$ is 1.4 times higher than in $\text{Ru}/\gamma\text{-Al}_2\text{O}_3\text{-ISO}$. Since changes in the CO_{ad} saturation coverage on that scale are unlikely, this points to an increase in surface area of the Ru NPs after the TPR sequence. Considering the little variation of the Ru NP size upon the TPR sequence, this would be consistent with the change in particle shape towards flat configurations, sufficient to overcompensate the loss of surface area due to the subtle increase in mean Ru particle size upon the TPR sequence.

FTIR spectra of the CO_{ad} region and fits of the individual contributions are presented in Figure 4. The pronounced bands at 2128 and 2078 cm^{-1} seem to be characteristic for CO_{ad} on the $\text{Ru}/\gamma\text{-Al}_2\text{O}_3\text{-TPR}$ catalyst, where their intensity is much higher than on $\text{Ru}/\gamma\text{-Al}_2\text{O}_3\text{-ISO}$. In contrast, the bands at 1974 and 2004 cm^{-1} and a weak contribution around 1950 cm^{-1} are characteristic for CO_{ad} on the $\text{Ru}/\gamma\text{-Al}_2\text{O}_3\text{-ISO}$ catalyst, where their intensities are much higher than for $\text{Ru}/\gamma\text{-Al}_2\text{O}_3\text{-TPR}$. The band at 2050 cm^{-1} shows about similar intensities on both catalysts, but considering the lower total

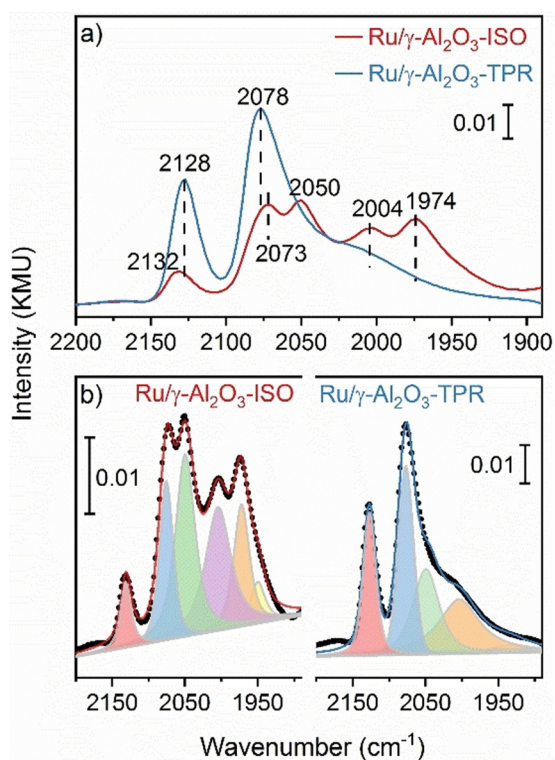


Figure 4. Ru particle shape analysis probed by in situ IR spectroscopy. a) DRIFT spectra showing the CO_{ad} band region of $\text{Ru}/\gamma\text{-Al}_2\text{O}_3\text{-ISO}$ and $\text{Ru}/\gamma\text{-Al}_2\text{O}_3\text{-TPR}$ catalysts. Spectra were recorded under steady-state conditions during low-temperature (30°C) CO adsorption from 1% CO/N_2 . b) Deconvolution of the spectra in (a).

CO_{ad} band intensity on $\text{Ru}/\gamma\text{-Al}_2\text{O}_3\text{-ISO}$ the relative contribution of the related CO_{ad} species is lower on the $\text{Ru}/\gamma\text{-Al}_2\text{O}_3\text{-TPR}$ catalyst.

Bands at $\approx 2130\text{ cm}^{-1}$ were assigned to Ru-multicarbonyl species adsorbed at undercoordinated Ru atoms, e.g., at the periphery interface sites of the Ru NPs, with more than one CO adsorbed on low-coordination Ru atoms.^[21,26,27] In a recent study, bands $\approx 2070\text{--}2080\text{ cm}^{-1}$ were assigned to asymmetric stretch vibrations of the above species and to CO on-top adsorbed on Ru sites that are electronically modified by interaction with the substrate (“monolayer sites”),^[21] e.g., sites at the interface perimeter.^[16,28] Bands in the range $2000\text{--}2050\text{ cm}^{-1}$ were associated with on-top CO adsorbed on Ru NPs,^[21,26,27] while bands below that range were attributed with bridge-bonded CO.^[28]

Based on the band intensities (Figure 4b), the fraction of the CO_{ad} species characteristic for the flat Ru NPs (bands at 2078 and 2132 cm^{-1}) increased from 23% for $\text{Ru}/\gamma\text{-Al}_2\text{O}_3\text{-ISO}$ to 49% for $\text{Ru}/\gamma\text{-Al}_2\text{O}_3\text{-TPR}$. The higher abundance of CO in multicarbonyl and monolayer Ru sites on the $\text{Ru}/\gamma\text{-Al}_2\text{O}_3\text{-TPR}$ catalyst is in perfect agreement with the conclusion derived from (S)TEM imaging that the Ru particles in the $\text{Ru}/\gamma\text{-Al}_2\text{O}_3\text{-TPR}$ catalyst are flatter and stabilized by stronger interaction with the modified substrate. In that case, we would expect an increase in island edges, the formation of a large fraction of “monolayer sites”, and a decrease of sites typical for hemispherical particles. The fact that there is some

intensity at 2130 and at 2070 cm^{-1} also on the $\text{Ru}/\gamma\text{-Al}_2\text{O}_3\text{-ISO}$ catalyst can simply be explained by the fact that also i) on this hemispherical catalyst undercoordinated sites exist at the periphery of the interface that can give rise to these CO_{ad} species and that ii) this catalyst also contains flat particles, but fewer and less pronounced. Correspondingly, the fraction of CO_{ad} species typical for CO adsorption on small hemispherical Ru NPs decreases upon the TPR sequence.

Next we examined the coordination of the Ru atoms in the Ru NPs during reaction by *operando* EXAFS measurements at the Ru K-edge. Fourier transforms of representative spectra in (SR-ref 6000) are shown in Figure 5a. Here it should be noted that the shorter reaction times during *operando* XAS measurements are still sufficient to essentially reach steady-state conditions (see details in Experimental section, SI). After calcination, the $\text{Ru}/\gamma\text{-Al}_2\text{O}_3$ catalyst showed a dominant Ru-O coordination shell at a distance of $2.2 \pm 0.1\text{ \AA}$, with Ru-O coordination numbers ($\text{CN}_{\text{Ru-O}}$) of 5.0 ± 0.5 (fit parameters in Table S3, SI). Upon switching to the reaction gas (190°C-1), the $\text{CN}_{\text{Ru-O}}$ decreased rapidly, being negligible already after 5 min, while the corresponding $\text{CN}_{\text{Ru-Ru}}$ values increased to 3.2 ± 0.5 and grew further to 5.7 ± 0.5 after 30 min on stream. For the remaining time at 190°C-1 it stayed constant. Hence, reduction of the oxidic Ru NPs to metallic Ru NPs occurs in the first few minutes during reaction. During the TPR sequence and the 190°C-2 phase, the $\text{CN}_{\text{Ru-Ru}}$ value remained unchanged at 5.5 ± 0.5 (Figure 5a and Figure S6, SI). Considering that the CN of Ru-Ru is determined by Ru particle size and shape, we would expect an increase in the CN for an increase in particle size and a decrease for a flattening of the particles. The constant $\text{CN}_{\text{Ru-Ru}}$ value upon the TPR sequence can be rationalized by a counterbalance between the small increase in mean particle diameter, from 1.5 to 1.7 nm, and the change in particle shape, from hemispherical to flat.

Further information on the chemical state of the Ru NPs was obtained from the XANES spectra (Figure 5b). The spectra recorded after calcination at 150°C show a strong white line contribution between 22120 and 22160 eV , whose shape is a combination of the RuO_2 and RuCl_3 references. Only 5 min after switching to the reaction gas, the white line intensity has decreased dramatically and then remained almost constant, consistent with a very fast reduction of most of the oxidic Ru species (Figure 5b and Figure S7, SI). Based on a linear combination analysis (LCA) of the XANES region for the $\text{Ru}/\gamma\text{-Al}_2\text{O}_3$ catalyst the freshly calcined catalyst is composed of $\approx 92\%$ oxidic and $\approx 8\%$ metallic Ru species (Figure 5c and Figure S8, SI). The contribution of metallic Ru species in the $\text{Ru}/\gamma\text{-Al}_2\text{O}_3$ catalyst increased to $\approx 83\%$ in the first 5 min reaction at 190°C-1 and further to $\approx 88\%$ at extended reaction times. During the TPR sequence, specifically at $300\text{--}350^\circ\text{C}$, the Ru species became even 100% metallic. However, after cooling back to 190°C , the content of metallic Ru species decreased slightly to $\approx 95\%$ during the first 40 min and then remained at this value. The slight re-oxidation fits well to the observed initial slight deactivation after the TPR sequence.

XPS measurements (Figure 5d and Figure S9, SI) revealed that the binding energies (BEs) of the main Ru $3d_{5/2}$

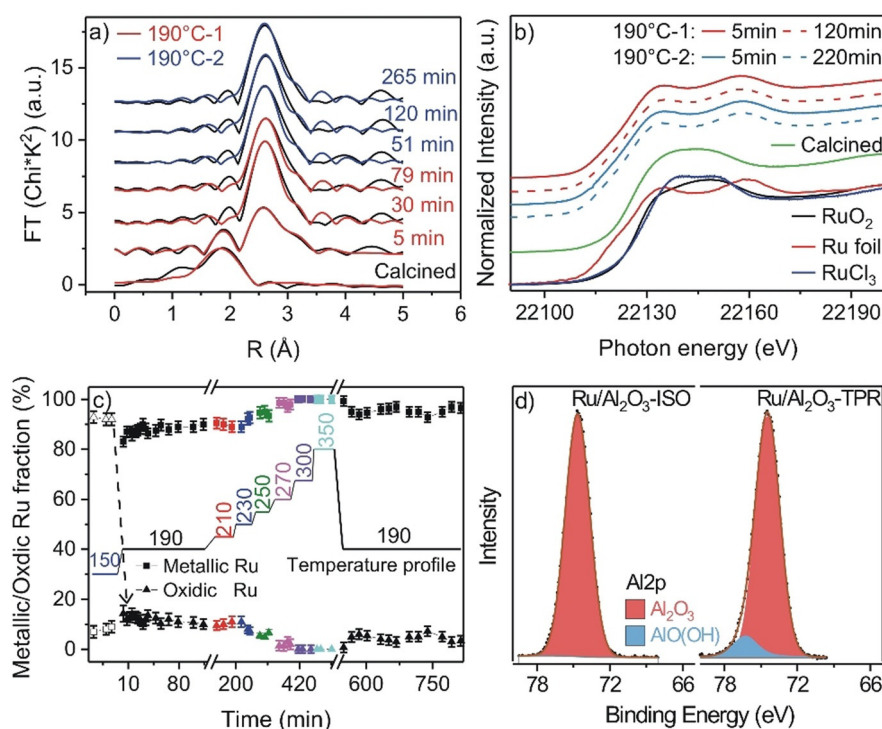


Figure 5. a) Fourier transformed EXAFS spectra in R-space recorded at the Ru K-edge in N₂ after calcination and at different reaction times on the Ru/γ-Al₂O₃ catalyst in SR-ref 6000 at 190°C (black lines: measured EXAFS data, red/blue lines: fit data (red: during 190°C-1, blue: during 190°C-2)). b) XANES spectra of references (Ru foil, RuO₂, RuCl₃ powder) and of the Ru/γ-Al₂O₃ catalyst in N₂ after calcination and during reaction in SR-ref 6000 at 190°C at different reaction times. c) Fractions of metallic Ru (square symbols) and oxidic Ru species (RuO₂ and RuCl₃; triangular symbols) as a function of time as derived from a LCA analysis of the XANES spectra of the Ru/γ-Al₂O₃ catalyst. d) XP spectra of the Al 2p region of the Ru/γ-Al₂O₃-ISO and Ru/γ-Al₂O₃-TPR catalysts, respectively. Note that the FWHM of the major Al 2p component of the Ru/γ-Al₂O₃-TPR was fixed at the same value of the Al 2p peak of the Ru/γ-Al₂O₃-ISO sample (FWHM = 2.35 eV).

component of the Ru/γ-Al₂O₃-ISO and -TPR catalysts are around 280.6 ± 0.1 eV, which in agreement with previous XPS data is slightly higher than the value of metallic Ru.^[6] Based on a deconvolution of Ru 3d spectra (Figure S10, SI), the contribution of surface metallic Ru species in the Ru/γ-Al₂O₃ catalyst is $\approx 80\%$ after 10 min reaction in the 190°C-1 phase, increasing to $\approx 87\%$ after 1000 min on stream. After the TPR sequence, the contribution of oxidic Ru is hardly visible any more ($\approx 91\%$ metallic Ru). These *ex situ* XPS results agree very well with the trend observed by *operando* XANES results (Figure 5c). The amount of surface carbon on the Ru/γ-Al₂O₃-ISO and -TPR catalysts, as evident from the C 1s signal at ≈ 284.8 eV, was essentially identical for both catalysts, indicating that the TPR sequence did not lead to increasing carbon deposition. For the Al 2p peak we obtained a BE of 74.6 ± 0.1 eV, which is typical for fully oxidized Al₂O₃.^[29] Interestingly the full width half maximum (FWHM) of the Al 2p peak for the Ru/γ-Al₂O₃-TPR catalyst (2.5 ± 0.05 eV) was significantly larger than that of the Ru/γ-Al₂O₃-ISO catalyst (2.35 ± 0.05 eV). Peak fitting of the Al 2p spectrum of the Ru/γ-Al₂O₃-TPR catalyst results in a good fit if we add a second component at about 76.3 eV with a FWHM = 2.35 eV, which comprises about 9.5% of the Al³⁺ ions in the γ-Al₂O₃-TPR catalyst. Following a previous assignment,^[30,31] we attribute this peak to aluminum oxyhydroxide (AlO(OH)) species. The discrepancy to the NMR

results can be explained by the surface sensitivity of XPS measurements.

Information on the adsorption properties of the Ru catalysts, basically CO_{ad} species and hydroxyl groups, was derived during reaction in SR-ref 6000 reformat and additionally in ID-ref 6000 reformat in the absence of CO₂ (Figure 6a,b). The ID-ref 6000 reformat was chosen to identify changes in the OH bands, which are not accessible in the presence of CO₂ due to interference with CO₂ combination bands ($3500\text{--}3800$ cm⁻¹). Note that the behavior of CO_{ad} species during reaction in ID-ref 6000 is almost identical to that in SR-ref 6000 (Figure S11–S12, SI). During the 190°C-1 phase, we observed bands at 3673 cm⁻¹ and at 3701 cm⁻¹, which had been assigned previously to hydrogen bonded OH and to bridged OH (b-OH) on sixfold coordinated Al sites (Al_{VI}) of γ-Al₂O₃ (110) facets.^[32,33] The intensity of these bands increased in the initial 20 min and then remained constant (Figure 6a). During the TPR sequence we only observed these H-bonded and bridged OH groups between 210 and 250°C (left panel in Figure S11, SI). At 270°C, a new band appeared at 3747 cm⁻¹, which has been calculated as characteristic for terminal OH (t-OH) on penta-coordinated Al (Al_V) sites of γ-Al₂O₃ (110) surfaces, but also for μ₃-type bridged OH (b-OH₁₁₁) on hexa-coordinated Al_{VI} sites of polar (111) facets.^[33] The relative concentration of this band increased with increasing temperature up to 350°C (left panel in Figure S11, SI). Since we cannot distinguish between

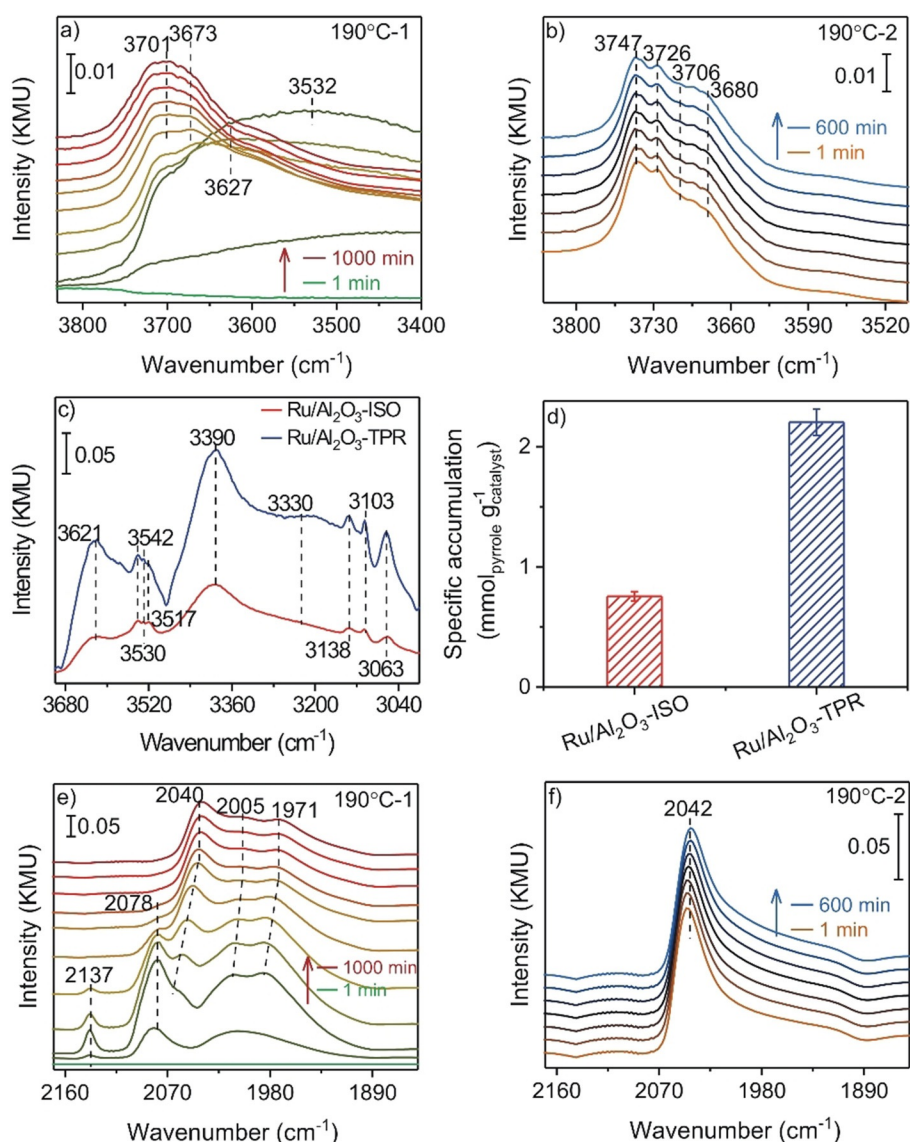


Figure 6. a),b) Time-resolved in situ DRIFT spectra of OH groups recorded at different times during reaction in ID-ref 6000 reformat at a) 190°C-1 (1, 2, 5, 7, 10, 20, 60, 120, 360, 660, 1000 min) and b) 190°C-2 (1, 60, 120, 240, 360, 480, 600 min). Note the intense and broad water bands (3500–3630 cm⁻¹) appearing during the initial reduction of the Ru oxide NPs. c) In situ DRIFT spectra of the different pyrrole covered Ru/γ-Al₂O₃ catalysts (steady-state conditions) at 30°C, d) accumulated, catalyst-mass-normalized amount of desorbed pyrrole during a TPD measurement in N₂. e),f) Time-resolved in situ DRIFT spectra of the CO_{ad} region recorded at different times during reaction in SR-ref 6000 at e) 190°C-1 phase (1, 2, 5, 7, 10, 20, 60, 120, 360, 660, 1000 min) (e) and f) 190°C-2 phase (1, 60, 120, 240, 360, 480, 600 min).

both species from the present data, we will henceforth denote them as OH_{TPR} species. The previously observed bands at 3673 and 3701 cm⁻¹ shifted to 3680 and 3706 cm⁻¹, respectively (Figure S11, SI). After cooling back to 190°C, the OH region was dominated by the band at 3747 cm⁻¹, a very small band at 3726 cm⁻¹ may point to water adsorbed on Al_v sites of the γ-Al₂O₃ surface (Figure 6b).^[33] Overall, these observations point to a distinct, activated modification of the Al₂O₃ surface during the TPR sequence, reflected by a change in the type of the dominant OH groups. Driving force for this change must be a higher stability of the resulting surface under TPR conditions, which, however, is maintained also during subsequent reaction at 190°C.

The t-OH groups were previously reported to possess a higher Lewis basicity (higher net charge) compared to the b-

OH groups.^[34] Therefore we tested whether the pronounced formation of the OH_{TPR} groups during the TPR sequence, at temperatures ≥ 270°C, will increase the Lewis basicity of the γ-Al₂O₃ support. This could enhance the interaction between Ru and Al₂O₃ and thus stabilize flat Ru NPs. We examined changes in the number and properties of Lewis basic sites (O²⁻, OH groups, etc.) of the γ-Al₂O₃ support upon the TPR sequence by pyrrole titration experiments. Here we focused on the N-H stretch vibration of adsorbed pyrrole.

The DRIFT spectra (Figure 6c) indicate a significantly higher concentration of Lewis basic sites (basic O²⁻ (≈ 3330–3390 cm⁻¹) and OH species (≈ 3621 cm⁻¹)) on the Ru/γ-Al₂O₃-TPR catalyst than on Ru/γ-Al₂O₃-ISO^[35,36] (detailed assignments see Section 12, SI). Analyzing the amount of gas phase pyrrole at the DRIFTS cell outlet during a temperature

programmed desorption (TPD) measurement by transmission IR spectroscopy (Figure S13, SI), we detected a roughly 3 times higher amount of pyrrole desorption from Ru/ γ -Al₂O₃-TPR (2.2 mmol_{pyrrole} g⁻¹_{catalyst}) than from the Ru/ γ -Al₂O₃-ISO catalyst (0.76 mmol_{pyrrole} g⁻¹_{catalyst}, Figure 6d and Figure S14, SI). Hence, the pyrrole titration confirms a significantly higher amount of Lewis basic sites (basic O²⁻ sites and OH groups) on the γ -Al₂O₃-TPR support. DFT calculations of the interaction of small Ru clusters with (100) and (110) γ -Al₂O₃ surfaces revealed that the introduction of surface OH groups enhances the basicity of the (100) surface, but lowers it for the (110) surface. This stabilizes the interaction between Ru and (hydroxylated) γ -Al₂O₃ for the (100) surface, while this is opposite for the (110) surface.^[20,37]

In combination, these results point to stronger interactions between the OH_{TPR} hydroxylated γ -Al₂O₃ and Ru NPs on the Ru/ γ -Al₂O₃-TPR catalyst compared to the b-OH hydroxylated Ru/ γ -Al₂O₃-ISO catalyst, resulting in a stabilization of flat Ru NPs after TPR sequence. So far we have not considered, however, that the OH_{TPR} type hydroxylation has to be present underneath the Ru NPs to result in a stronger interaction. In a static system these surface areas are not accessible to gas phase species. Hence, the higher temperatures during the TPR sequence are not only required to activate the reaction between γ -Al₂O₃ surface and gas phase, but also to enhance the mobility of the Ru NPs to an extent that these can move to modified surface areas, where they are stabilized by the stronger interactions between modified surface and Ru NPs. The enhanced mobility of the Ru NPs also allows the thermodynamically favored reshaping of the Ru NPs.

In the C-O stretch region, there are significant differences in the CO_{ad} bands between the DRIFT spectra recorded during reaction (Figure 6e,f) and during CO adsorption at 30 °C (Figure 4). During the 190 °C-1 phase, the “Ru monolayer” species at \approx 2078 cm⁻¹ appeared only during the first 1 h reaction and vanished after that, the small band at 2137 cm⁻¹ had disappeared after few min. The on-top CO_{ad} species characteristic for the hemispherical Ru NPs, which under reaction conditions appears at 2040 cm⁻¹, and the bridge bonded CO_{ad} species at 1971 cm⁻¹ were almost unchanged for over 1000 min. Considering the much higher temperature during reaction than during the CO adsorption experiment in Figure 4, the complete absence of the high frequency bands under reaction conditions indicates that the multicarbonyl and “Ru monolayer” CO_{ad} species with bands at 2132 and 2078 cm⁻¹, respectively, relate to less strongly bound CO_{ad} species.

During the TPR sequence, the CO_{ad} coverage decreased due to the higher CO and CO₂ conversion and desorption under these conditions; in addition, the CO_{ad} bands also red shifted due to the lower CO-CO repulsion/ dipole-dipole coupling at lower CO_{ad} coverages (right panel in Figure S11, SI). After cooling back to 190 °C, we observed only the band of on-top CO_{ad} at 2042 cm⁻¹, while the low frequency CO_{ad} bands almost disappeared. Furthermore, the total intensity is significantly lower, by 47%, than before the TPR sequence. This discrepancy to the behavior during low-temperature CO adsorption (Figure 4), where the TPR sequence leads to an

increase of CO_{ad} coverage, can be explained by the significantly weaker bonding of CO in the multicarbonyl and the “monolayer Ru” CO_{ad} states with their bands at 2132–2137 and 2078 cm⁻¹, respectively, discussed above. During low-temperature CO adsorption, these sites are saturated with CO_{ad}, while they are little populated under reaction conditions at 190 °C. This leads to a strong reduction of the total CO_{ad} coverage during reaction on the Ru/ γ -Al₂O₃-TPR catalyst, while on the Ru/ γ -Al₂O₃-ISO catalyst the contribution of multicarbonyl and Ru monolayer CO_{ad} sites is much smaller, and therefore its steady-state coverage is less affected. Furthermore, the significantly higher reaction rate on the Ru/ γ -Al₂O₃-TPR catalyst may also modify the occupation of different sites. For comparison, we also performed a blank experiment, monitoring the evolution of the adsorbate layer on a pure γ -Al₂O₃ support in SR-ref 6000 reformat gas by in situ DRIFTS measurement. They only show the gas phase signals of the reactants CO and CO₂ (Figure S15, SI).

Furthermore, not only CO/CO₂ adsorption and reaction are modified by the TPR sequence, but also the hydrogen adsorption/ desorption behavior. Exposing the catalysts to a mixture of H₂ and D₂ (10% H₂/ 10% D₂/N₂, 190 °C), the amount of HD formation was significantly higher (about 20%) over the Ru/ γ -Al₂O₃-TPR catalyst than over the Ru/ γ -Al₂O₃-ISO catalyst on the flat Ru NPs (Figure S16, SI).

Finally we would like to note that, although γ -Al₂O₃ is considered to be very stable and non-reducible, the present data clearly demonstrate that a reductive treatment can modify its metal-support interactions, a phenomenon which so far had been reported only for noble metal NPs supported on reducible oxides.^[15]

Conclusion

In combination, these data indicate that the high-temperature treatment during CO_x methanation activates two processes that are kinetically hindered at lower temperatures: First, they activate the reactive modification of the support, leading to the formation of OH_{TPR} species on its surface. Second, they activate the mobility of the Ru NPs, allowing them to transfer to already modified adjacent support sites. This first step results in the formation of Lewis basic sites on the γ -Al₂O₃ surface with an enhanced interaction between Ru and γ -Al₂O₃, which can stabilize flat Ru NPs, while the second part describes the kinetic activation required for the structural transformation of the Ru NPs. In total, we demonstrate that the enhanced MSIs induced by the temperature programmed reaction sequence result in a drastic increase of the CO₂ methanation activity of the Ru/ γ -Al₂O₃ catalyst, both in the absence and presence of CO traces. This way Ru/ γ -Al₂O₃ reaches the activity of highly active Ru based catalysts, while keeping a high stability. Such kind of reductive higher-temperature treatment provides a simple approach to fabricate a highly active and stable catalyst for methanation reactions, which can be useful for a wide range of reactions based on these supports.

Acknowledgements

S.C. is grateful for a fellowship from the Ministry of Science, Research and Arts of the State of Baden-Württemberg. We acknowledge the electron synchrotron facilities Petra-III (DESY, Germany, P65 beamline) and Elettra Sincrotrone (Trieste, Italy, XAFS beamline) for the provision of beam time and technical assistance. Finally, we would like to thank Dr. T. Diemant and S. Blessing (Ulm University) for XPS and XRD measurements. The Institute of Engineering Materials and Biomaterials of the Silesian University of Technology is acknowledged for the access to the Titan FEI TEM instrument. S.C., A.M.A., and J.B. are grateful for travel support for the synchrotron measurements by DESY (user office at DESY) and by Elettra (program CALIPSOplus, funded by Horizon 2020 EC program (GA n. 730872)). Open access funding enabled and organized by Projekt DEAL.

Conflict of interest

The authors declare no conflict of interest.

Keywords: CO₂ methanation · Lewis basic sites · Metal-support interactions · operando spectroscopy · particle shape

- [1] F. Schüth, *Chem. Ing. Tech.* **2011**, 83, 1984.
- [2] M. Götz, J. Lefebvre, F. Mörs, A. McDaniel Koch, F. Graf, S. Bajohr, R. Reimert, T. Kolb, *Renewable Energy* **2016**, 85, 1371.
- [3] C. Vogt, M. Monai, G. J. Kramer, B. M. Weckhuysen, *Nat. Catal.* **2019**, 2, 188.
- [4] W. Wang, S. Wang, X. Ma, J. Gong, *Chem. Soc. Rev.* **2011**, 40, 3703.
- [5] P. Munnik, M. E. Z. Velthoen, P. E. de Jongh, K. P. de Jong, C. J. Gommers, *Angew. Chem. Int. Ed.* **2014**, 53, 9493; *Angew. Chem.* **2014**, 126, 9647.
- [6] S. Chen, A. M. Abdel-Mageed, C. Gauckler, S. E. Olesen, R. J. Behm, *J. Catal.* **2019**, 373, 103.
- [7] S. Kattel, P. Liu, J. G. Chen, *J. Am. Chem. Soc.* **2017**, 139, 9739.
- [8] S. Takenaka, T. Shimizu, K. Otsuka, *Int. J. Hydrogen Energy* **2004**, 29, 1065.
- [9] F. Wang, S. He, H. Chen, B. Wang, L. Zheng, M. Wei, D. G. Evans, X. Duan, *J. Am. Chem. Soc.* **2016**, 138, 6298.
- [10] A. M. Abdel-Mageed, K. Wiese, M. Parlinska-Wojtan, J. Raebach, A. Brückner, R. J. Behm, *Appl. Catal. B* **2020**, 270, 118846.
- [11] A. M. Abdel-Mageed, D. Widmann, S. E. Olesen, I. Chorkendorff, R. J. Behm, *ACS Catal.* **2018**, 8, 5399.
- [12] S. Chen, A. M. Abdel-Mageed, D. Li, J. Bansmann, S. Cisneros, J. Biskupek, W. Huang, R. J. Behm, *Angew. Chem. Int. Ed.* **2019**, 58, 10732; *Angew. Chem.* **2019**, 131, 10842.
- [13] S. J. Tauster, S. C. Fung, R. L. Garten, *J. Am. Chem. Soc.* **1978**, 100, 170.
- [14] M. Ahmadi, H. Mistry, B. Roldan Cuenya, *J. Phys. Chem. Lett.* **2016**, 7, 3519.
- [15] T. W. van Deelen, C. Hernandez Mejia, K. P. de Jong, *Nat. Catal.* **2019**, 2, 955.
- [16] Z. Liu, F. Zhang, N. Rui, X. Li, L. Lin, L. E. Betancourt, D. Su, W. Xu, J. Cen, K. Attenkofer, H. Idriss, J. A. Rodriguez, S. D. Senanayake, *ACS Catal.* **2019**, 9, 3349.
- [17] T. Abe, M. Tanizawa, K. Watanabe, A. Taguchi, *Energy Environ. Sci.* **2009**, 2, 315.
- [18] S. Li, Y. Xu, Y. Chen, W. Li, L. Lin, M. Li, Y. Deng, X. Wang, B. Ge, C. Yang, S. Yao, J. Xie, Y. Li, X. Liu, D. Ma, *Angew. Chem. Int. Ed.* **2017**, 56, 10761; *Angew. Chem.* **2017**, 129, 10901.
- [19] J. H. Kwak, J. Hu, D. Mei, C. W. Yi, D. H. Kim, C. H. F. Peden, L. F. Allard, J. Szanyi, *Science* **2009**, 325, 1670.
- [20] J. Yang, X. Zhao, S. Bu, W. Fan, *J. Phys. Chem. C* **2018**, 122, 17287.
- [21] Y. Yan, Q. Wang, C. Jiang, Y. Yao, D. Lu, J. Zheng, Y. Dai, H. Wang, Y. Yang, *J. Catal.* **2018**, 367, 194.
- [22] S. Eckle, H.-G. Anfang, R. J. Behm, *Appl. Catal. A* **2011**, 391, 325.
- [23] A. M. Abdel-Mageed, S. Eckle, H.-G. Anfang, R. J. Behm, *J. Catal.* **2013**, 298, 148.
- [24] P. Panagiotopoulou, D. I. Kondarides, X. E. Verykios, *Appl. Catal. B* **2009**, 88, 470.
- [25] A. M. Abdel-Mageed, D. Widmann, S. E. Olesen, I. Chorkendorff, J. Biskupek, R. J. Behm, *ACS Catal.* **2015**, 5, 6753.
- [26] K. Hadjiivanov, J.-C. Lavalley, J. Lamotte, F. Maugé, J. Saint-Just, M. Che, *J. Catal.* **1998**, 176, 415.
- [27] B. T. Loveless, C. Buda, M. Neurock, E. Iglesia, *J. Am. Chem. Soc.* **2013**, 135, 6107.
- [28] S. Y. Chin, C. T. Willimas, M. D. Amiridis, *J. Phys. Chem. B* **2006**, 110, 871.
- [29] J. F. Moulder, W. F. Stickle, P. E. Sobol, K. D. Bomben, *Handbook of X-ray Photoelectron Spectroscopy* (Ed.: J. Chastain), PerkinElmer Corp., Eden Prairie, USA, **1992**.
- [30] J. T. Klopogge, L. V. Duong, B. J. Wood, R. L. Frost, *J. Colloid Interface Sci.* **2006**, 296, 572.
- [31] J. S. Corsi, J. Fu, Z. Wang, T. Lee, A. K. Ng, E. Detsi, *ACS Sustainable Chem. Eng.* **2019**, 7, 11194.
- [32] G. Busca, V. Lorenzelli, S. Escribano, R. Guidelli, *J. Catal.* **1991**, 131, 167.
- [33] M. Digne, P. Sautet, P. Raybaud, P. Euzen, H. Toulhoat, *J. Catal.* **2004**, 226, 54.
- [34] C. Morterra, G. Magnacca, *Catal. Today* **1996**, 27, 497.
- [35] P. O. Scokart, P. G. Rouxhet, *J. Chem. Soc. Faraday Trans.* **1980**, 76, 1476.
- [36] J. C. Lavalley, *Catal. Today* **1996**, 27, 377.
- [37] J. Yang, H. Wang, X. Zhao, Y. L. Li, W. L. Fan, *RSC Adv.* **2016**, 6, 40459.

Manuscript received: May 19, 2020

Accepted manuscript online: August 4, 2020

Version of record online: October 7, 2020